https://doi.org/10.3311/PPme.22672

Periodica Polytechnica Mechanical Engineering, 68(4), pp. 279–290, 2024

Assessing the Effect of Uneven Inlet Velocity on the 24 ft Diameter MinwaterCSP Fan Using a Unique Pressure Sensing System

Cesar C. Thiry[1], Sybrand J. van der Spuy[1*], Giovanni Delibra[2], Lorenzo Tieghi[2]

[1] Department of Mechanical and Mechatronic Engineering, Stellenbosch University, 7602 Matieland, P.O.B. X1, South Africa
[2] Department of Mechanical and Aerospace Engineering, Sapienza University of Rome, via Eudossiana 18., 00184 Rome, Italy
[*] Corresponding author, e-mail: sjvdspuy@sun.ac.za

Received: 28 May 2023, Accepted: 06 November 2024, Published online: 13 November 2024

Abstract

An industrial-grade pressure sensing system was designed for installation on the surface of the 24 ft (7.315 m) diameter M-fan that is installed on the MinwaterCSP test facility. The facility has significant cross draft effects due to the proximity of a canal that runs underneath the centre of the facility. This canal causes disturbance of the inlet air flow distribution. Due to the constant rapid change in air velocity and direction with blade rotation, the pressure on the blade fluctuates. The velocity distribution was measured experimentally using the installed anemometers. The uneven inlet velocity distribution led to fluctuations in blade surface pressures, which were measured using the uniquely designed pressure sensing system. The measured results were compared to the results of a Computational Fluid Dynamics (CFD) model of the MinwaterCSP test facility. The CFD simulations consisted of two parts. Firstly a 3-dimensional representation of the facility, which was used to get the velocity distribution data and secondly a 2-dimensional airfoil simulation which was used to obtain the surface pressure distribution on the blade surface. The 3-dimensional CFD model made use of an actuator disk model to represent the effect of the fan. The experimental results showed a higher velocity and relative surface pressure distribution at locations correlating to the location of the canal. The simulation was able to replicate these distribution fluctuations. The results of the experimentally measured fan blade surface pressure at the fan suction side correlated within 9% to those of the simulation results.

Keywords

axial flow fan, air-cooled condenser, ACC, blade surface pressure

1 Introduction

Wet-cooling is the largest contributor to water consumption in a typical concentrating solar power (CSP) plant. Therefore, the European Union Horizon 2020 program funded the MinwaterCSP project to develop solutions to reduce cooling system water consumption and auxiliary power consumption in concentrating solar power plants [1]. Due to the arid nature of typical CSP environments and the stricter regulatory constraints on the use of water for industrial cooling, an increasing trend towards the use of forced draught dry-cooling is observed [2]. The MinwaterCSP test facility (see Fig. 1) was constructed to test the components of such a cooling system [3]. For this purpose, it is equipped with a 24 ft (7.315 m) diameter axial flow M-fan to drive air through the facility.

The M-fan was designed to meet the requirements of a high design flow rate and low pressure rise, associated with current large diameter cooling fans [4]. The fan design process is described by Wilkinson et al. [5] and is based on the work of Louw et al. [6]. The details of the M-fan design are shown in Table 1.

As can be seen from Fig. 1, a canal runs underneath the MinwaterCSP test facility, and it is expected to have a noticeable effect on the fan inlet velocity distribution. This may further cause a disturbance in fan blade surface pressure distribution over the rotation plane of the fan [7].

This investigation considers a cost-effective method for retrofitting pressure sensing attachments to the outer surface of an existing, installed fan for determining its performance. The attachments are designed in such a manner that they do not impede the performance of the fan and are simultaneously capable of sending data over a data network. A concept pressure sensing system, previously

Cite this article as: Thiry, C. C., van der Spuy, S. J., Delibra, G., Tieghi, L. "Assessing the Effect of Uneven Inlet Velocity on the 24 ft Diameter MinwaterCSP Fan Using a Unique Pressure Sensing System", Periodica Polytechnica Mechanical Engineering, 68(4), pp. 279–290, 2024. https://doi.org/10.3311/PPme.22672

Table 1 M-fan design characteristics [3]

Diameter	24 ft (7.315 m)
Number of blades	8
Hub-to-tip ratio	0.29
Fan rotational speed	151 rpm
Design flow rate	333 m^3/s
Design fan static pressure	116.7 Pa
Design fan shaft power	63.290 kW
Design fan static efficiency	61.4%
Flow coefficient (ϕ)	0.15
Fan static pressure coefficient (ψ)	0.058
Tip Reynolds number	3.14×10^6
Blade profile	NASA LS 0413

Fig. 1 Photo of the MinwaterCSP test facility

designed by Thiry [8], was therefore adapted and installed at specific measurement positions. A microcontroller, which performs the processing and conversion of the measured data to allow telemetry communication, was placed on the hub of the fan to minimize the effect of centrifugal forces exerted by fan rotation.

The paper details the experimental testing and Computational Fluid Dynamics (CFD) analysis of the fan inside the test facility. It compares the measured and analysed velocity and blade surface pressure distribution over the fan rotation plane. The goal was to experimentally determine the influence from the environment in the vicinity of the test facility and to determine if the simulation model could reproduce similar results. To the authors' knowledge, this is the first time that such pressure measurements have been performed on an installed, large diameter cooling fan. It should be noted that a particular challenge for these cooling fans is the process of measuring pressures in the range of 10 to 500 Pa. All results are shown at a nominal blade angle of 34° and at the maximum rotational velocity of the fan of 151 RPM.

The paper is divided into 5 parts. Section 1 shows the MinwaterCSP test facility lay-out. Secondly the experimental configuration is described, followed by an explanation of the numerical investigation used to analyse the installed 24 ft M-fan. Fourthly the investigation of the two- dimensional airfoil is shown, with the results from the experimental and numerical investigation presented and compared in the final fifth part.

The comparison between the experimental and numerical results is analysed, in order to report on the feasibility of the developed experimental set-up for measuring the installed fan performance.

2 Facility lay-out

The experiments were performed in the MinwaterCSP cooling system test facility at Stellenbosch University, South Africa (see Fig. 2). Due to the presence of several surrounding buildings the diameter of the installed fan in the facility was limited to 24 ft (7.315 m).

2.1 General system lay-out

It is expected that the facility will experience cross draft effects since it is constructed across a canal that runs underneath its center (1). The circular bell mouth inlet (2) and the square fan discharge plenum chamber (3) and louvres (4) to control the air flow through the facility are located above the canal [3].

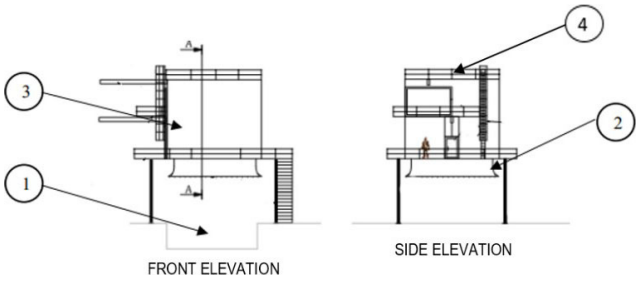

Fig. 2 Schematic of experimental facility. Adapted from [3]

2.2. Fan installation

The installed fan runs inside the bell mouth inlet. The area between the structural hub and fan blade roots are covered with a flat plate for aerodynamic purposes. A 132 kW electric motor with a 10:1 reduction gearbox is connected to the suspended fan rotor. The facility allows the fan rotor to run at a maximum speed of 151 rpm by means of a variable speed drive.

The entire MinwaterCSP test facility is controlled through a Siemens Programmable Logic Controller (PLC). The operator controls the PLC through a Supervisory Control and Data Acquisition (SCADA) system that is installed on a personal computer located inside the control room. The fan installation is shown in Fig. 3.

3 Experimental configuration

The facility has multiple measurement systems. Both the inlet and outlet of the facility are equipped with four fan-assisted psychrometers to measure the inlet and outlet wet and dry bulb temperatures. Propeller anemometers are installed on a rotating beam to measure the flowrate passing through the bell mouth inlet (these are further discussed in Section 3.3). A load cell is connected to a torque arm to measure the torque exerted by the fan drive, coupled with an optical speed pick-up to determine the fan running speed and consequently the fan shaft power. A set of pressure taps measure the pressure in the plenum chamber and are used to record the atmospheric pressure before running a test. Outlet propeller anemometers are used to monitor the flow distribution through the test facility during deluge tests.

3.1 Fan blade setting angle and tip clearance

The fan blades of the MinwaterCSP facility are equipped with an indexing system at the root of the blades that allow the fan blade angle to be adjusted at set 1° intervals. For this project the blade root angle was set to a nominal value of 34° relative to the plane of rotation. Each blade of the 8 bladed 24 ft M-fan was inspected and adjusted to have the correct fan blade angle at the root and the tip. The blade tip clearance was measured for each blade at 8 different locations along the circumference of the fan casing rotor. Table 2 shows the summary of these results.

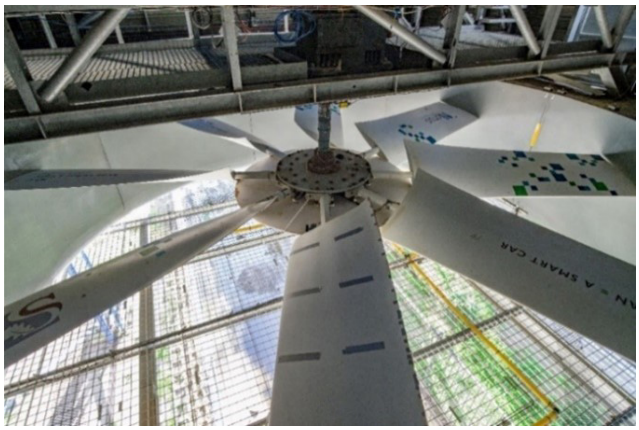

Fig. 3 Photo of the installed 24 ft M-fan

3.2 Rotational speed and shaft torque measurement

An optical sensor is used to measure the rotational speed of the M-fan in the MinwaterCSP facility. A reflective band is held stationary while an optical sensor rotates with the rotor shaft resulting in the rotational speed being computed and parsed through to the SCADA software.

The entire fan drive (motor and gearbox) lies on a slew bearing. The torque on the fan shaft is therefore measured by means of a load arm that connects an LT200 Load Tech loadcell to the gearbox. The loadcell has an accuracy of 0.1% (see Table 3). The measured load is multiplied by the arm length to obtain the torque exerted by the fan drive on the fan shaft. The fan shaft power is calculated by multiplying the shaft torque with the rotational speed.

3.3 Flowrate measurement

The flowrate passing through the inlet screen upstream of the installed fan is measured by means of six propeller anemometers installed at set distances along the length of an aluminium beam (see Fig. 4). The beam is rotated in intervals for a full 360° sweep with the use of a stepper motor to map the entire inlet flow field of the fan.

The anemometers measure the velocity of the air passing through it and translates it as a voltage value to a 16 channel QuantumX MX1601 where CATMAN software is used to apply the calibration factor and record the velocity data. The anemometers were individually calibrated in a dedicated calibration tunnel, with an inlet area of 0.234 m^2 to an accuracy within 2% (see Table 3 and Fig. 5) [9].

Table 2 24 ft M-fan installed blade properties

Blade stagger angle at hub	34° (nominal)
Blade stagger angle at tip	8.91° (SD = 0.34°)
Average blade tip clearance	0.27% (SD = 0.028%)

Table 3 Summary of quoted instrumentation accuracy values

Component	Accuracy
Torque arm loadcell accuracy	1%
Anemometer accuracy	2%
Pressure sensor accuracy	0.8%

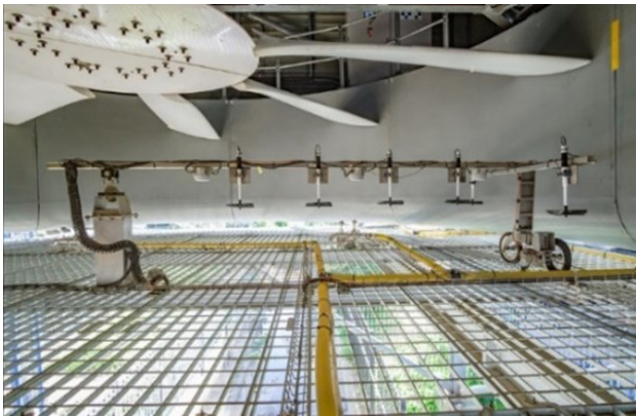

Fig. 4 Anemometers on rotating beam

Fig. 6 shows the anemometer experimentally measured air flow velocity, vm obtained by using a constant calibration factor of 1.76×10^{-2} multiplied with the measured voltage from anemometer, V_{an}, against the calculated airflow velocity, v_c:

$$v_m = 1.76 \times 10^{-2} \times V_{an}. \quad (1)$$

Each of the six anemometers, named from a to *f* in Fig. 7, occupy their own segment in a sector. Each anemometer segment area is calculated using the inner and outer radius of its segment and a set angle of 22.5°. An evaluation of the measurements shows that the average effect on the values caused by the difference in area between that of the calibration tunnel and the above segment is less than 0.1%. The anemometer beam is moved sequentially to possitions 1 through 16 (see Fig. 7). Once the anemometer beam is moved to its next position and stabelized, the velocity measurements are taken over a fixed time period. The average measured velocity is then multiplied by its corresponding segment area and added to obtain the flow rate through the fan inlet. Tests were performed at a set operating point of 151 RPM, 100% open louvre setting.

The directional sensitivity of the anemometers was investigated by Muiyser [9] and their accuracy was found to be within 5% when the air flow is within 40° of the measurement axis which is more than the anemometer is expected to be subjected to when placed below the fan.

Fig. 5 Propeller anemometer calibration in wind tunnel

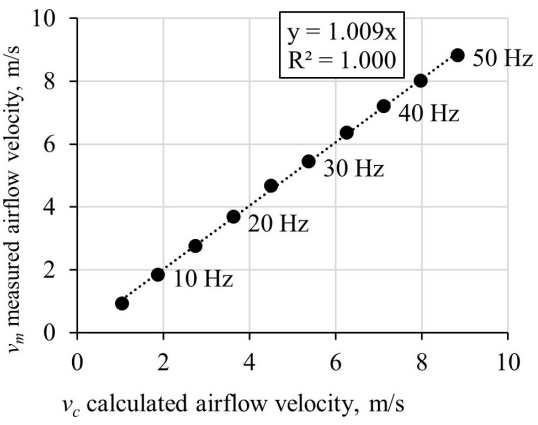

Fig. 6 Comparison of calculated and calibrated anemometer air flow velocity

3.4 Pressure sensing system

An LPS25HB absolute pressure sensor with a range of 260 to 1260 hPa and accuracy of within 10 Pa (see Table 3) was used for this study. The sensor is connected on a breakout board with a dimension of 25.4 × 50.8 mm and a thickness of 2 mm and connection pin being 8 mm thick. Through the connection pin the pressure sensor was plugged into an Arduino Uno microcontroller for further processing of the measured signal.

The pressure sensor was tested in the small wind tunnel facility at Stellenbosch University. The sensor was mounted on a flat plate at 30 mm from the leading edge (see Fig. 8). The values measured using the sensor were compared to values measured using a standard pressure tap and Betz manometer at the exact same distance from the plate leading edge. The results showed a standard

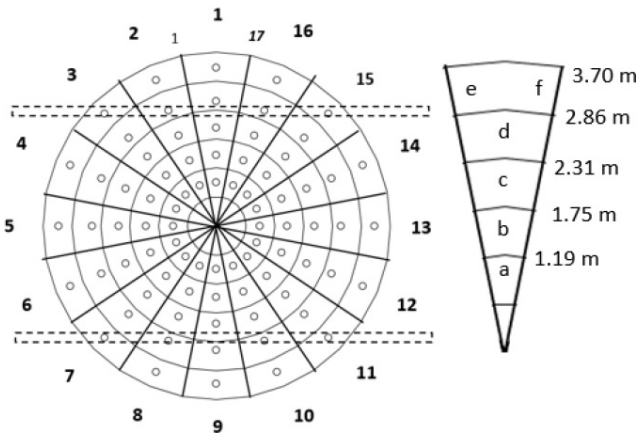

Fig. 7 Anemometer map of flow field

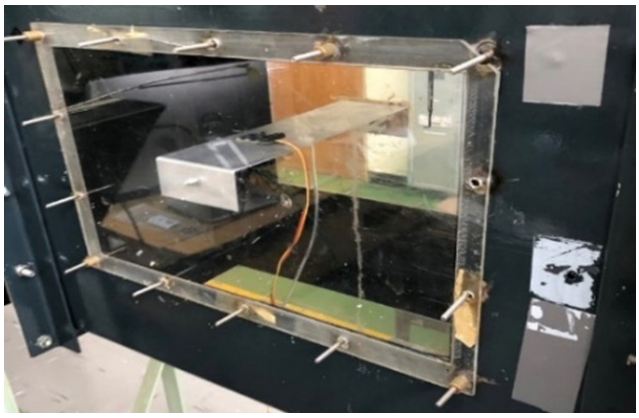

Fig. 8 Comparative measurements in small wind tunnel

deviation of 8 Pa for the values read by the sensor, when compared to the Betz manometer reading.

The pressure sensing system was installed on the M-fan in the MinwaterCSP facility to obtain the blade surface static pressures. One perceived advantage of the system is that it is "stick-on" and that it does not require special manufactured blades or parts (see Fig. 9).

The Arduino UNO and NANO microcontrollers on the signal and receiving ends of the system were connected to two XBee-PRO S2C Modules. The Arduino UNO microcontroller is the heaviest component in the system and therefore it was neatly fastened onto the central hub plate of the fan (see Fig. 10).

Alongside the microcontroller, its 9 V power unit was fastened with screws. All wires were flattened and held in place behond the blade's trailing edge using hot glue and duct tape. For the purpose of this investigation, the LPS25HB pressure sensors were installed at three different locations on the blade. Two positions were located on the suction side of the fan and one on the pressure side (see Fig. 11). Sensors 1 and 3 were positioned at a distance of 790 mm from the blade tip and 290 mm from the leading edge but on opposite sides of the fan blade, while sensor 2 was positioned at a distance of 1310 mm from the tip

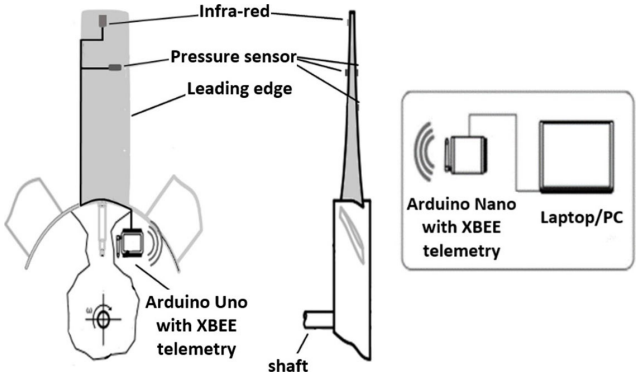

Fig. 9 Schematic representation of pressure sensing system

Fig. 10 Arduino microcontroller installation

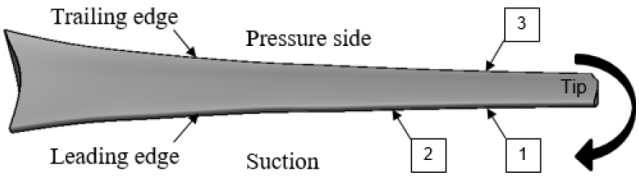

Fig. 11 Sensor positioning schematic

and at a similar distance of 290 mm from the leading edge on the suction side of the blade.

Fig. 12 shows the mounted sensors and cables on the blade. An infra-red sensor was installed on the blade and was used to measure the rotational velocity and consequently the sensor angular position in the rotational plane.

4 Numerical investigation

A Computational Fluid Dynamics (CFD) analysis of the installed 24 ft M-fan was performed in ANSYS Fluent® [10]. The purpose of the analysis was to simulate the performance of the fan in the MinwaterCSP facility. The results of this simulation were compared to the measured pressure and flow data, in order to assess the feasibility of the proposed measurement system.

The fan is modelled using an Actuator Disk Model (ADM). The ADM was originally derived by Thiart and von Backström [11] and uses blade element theory to calculate the momentum forces induced into the flow field by the fan rotor.

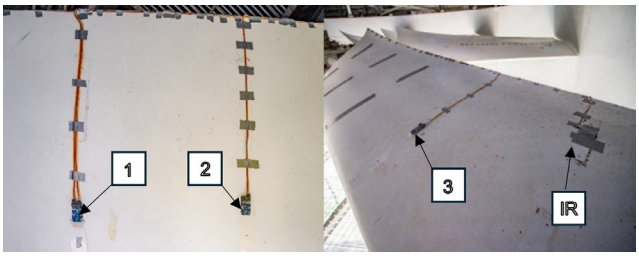

Fig. 12 Sensors mounted on the blade surface

In the ADM, the fan rotor is represented by an annular disk, being a single cell thick. The centre of this annular disk correlates to the mid-plan of the fan rotor. A User Defined Function (UDF) is used to calculate and introduce the momentum sources terms in the cells of the so-called rotor disk as:

$$F_z = L\cos\beta_\infty - D\sin\beta_\infty, \tag{2}$$

$$F_\theta = L\sin\beta_\infty + D\cos\beta_\infty, \tag{3}$$

where F_z and F_q are the momentum forces in the axial and tengential directions respectively, L and D represent the lift and drag force exerted by the particular blade element on the flow and β_∞ is the flow angle of the average velocity vector, relative to the plane of rotation. The average velocity vector is obtained from two annular disks, each being one chord length upstream and downstream of the central disk respectively.

The ADM is computationally efficient (compared to modelling a fan rotor in full detail) and has therefore been successfully used to model arrays of large diameter cooling fans in air-cooled condensers. As such, its use in this investigation is highly relevant. The standard k-ε turbulence model was found to work well when simulating a fan with an actuator disk in the study by Meyer and Kröger [12]. In the presence of rotating flow Shih et al. [13] promotes the use of a realizable k-ε model.

4.1 3D Computational grid and boundary conditions

Fig. 13 shows a schematic of the MinwaterCSP test facility. Important features to notice are that the facility is placed over a canal, with buildings located on either side thereof. These two features are expected to influence the resulting flow conditions through the fan. The simulation model depicted by Fig. 13 is an approximate representation of the MinwaterCSP test facility.

The current mesh has 5.5 million mesh elements with a minimum orthogonal quality of 0.16 and an average value of 0.78. The actuator disk was meshed with hexahedral elements having 70 radial intervals and 480 circumferential intervals. A sphere of influence was added around the actuator disk for better mesh interfacing with a mesh growth rate from the actuator disk outwards. Fig. 14 represents the meshing of the MinwaterCSP model. As seen in Fig. 14 a porous zone is positioned downstream of the actuator disk.

This porous medium model was incorporated to mimic the pressure drop over the 20 mm thick walking grid section present in the MinwaterCSP test facility. The pressure

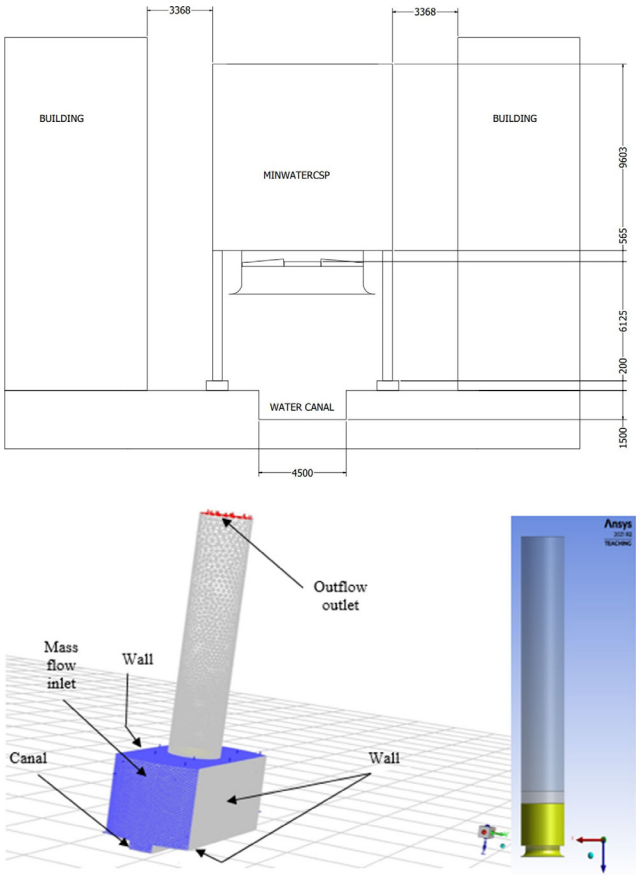

Fig. 13 CFD model of the MinwaterCSP test facility and CFD model without the surrounding environment

loss through the porous zone is modelled as source terms in the Darcy-Forchheimer equation:

$$\frac{\partial p}{\partial z} = -\frac{\mu}{K}V - \frac{\mu}{K_1}V^2, \tag{4}$$

with an inertial resistance factor of 2.442 m^{-1} and a viscous resistance factor of 1.173 × 10^{-6} m^{-2} both acting in the axial direction against the flow. Resistance factors are extracted from a previous study of van der Spuy and von Backström [14].

5 Two-dimensional airfoil investigation

A 2D airfoil investigation was performed to investigate the surface pressure distribution on the fan blade element. The current investigations were performed to compare the fluctuation in surface pressure due to the installed effects present in the MinwaterCSP facility caused by the canal and buildings. Two airfoil profiles had to be simulated to correspond to the pressure sensor positions 1, 2 and 3. Data about the angle of attack and velocities were gathered from the 3-dimensional simulation to calculate the relative velocity needed for the 2D simulation. This was

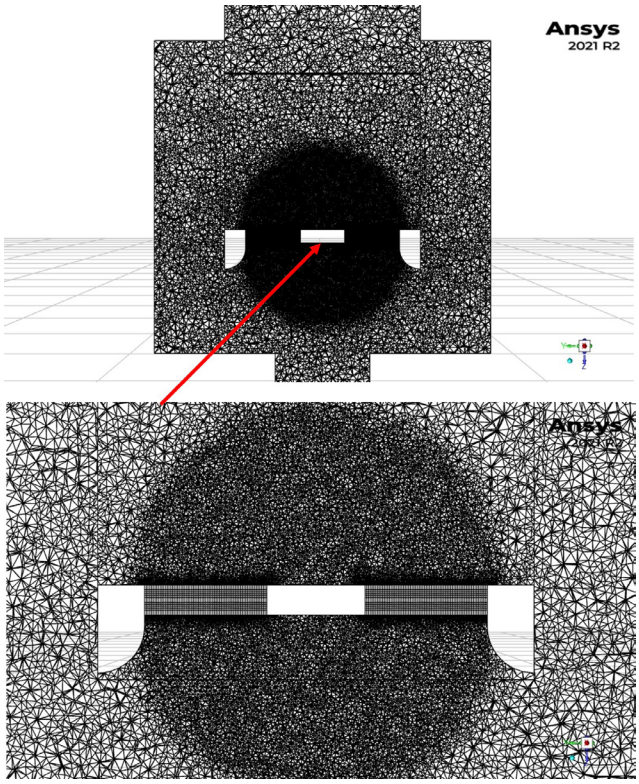

Fig. 14 Y-Z plane cut of mesh lay-out with zoomed-in view of actuator disks and sphere of influence mesh attribute

performed at 8 different locations, every 45° in the actuator disk plane. The calculated different reference velocities allowed the 2D airfoil to be simulated and to obtain different surface pressures which could be compared to those gathered experimentally. The relative velocity vector of a two-dimensional blade element is calculated as the average between the up- and downstream velocity vectors of the 2D blade element [13].

5.1 Computational description

A three-dimensional picture of the M-fan blade as design by Wilkinson et al. [5] is shown in Fig. 15.

A radial cut was taken at 2868 mm and 2348 mm from the hub centre and unwrapped to have the radial two-dimensional airfoil profile as shown in Fig. 16.

5.2 Computational domain and mesh

The computational grid only used quadrilateral mesh elements. This allowed for better mesh element fitting around the airfoil profile (Fig. 17). To solve the boundary layer accurately the cells near the airfoil surface have been refined such that $y^+ \sim 1$, in line with the requirements of the turbulence model. A total of 2 million quadrilateral mesh

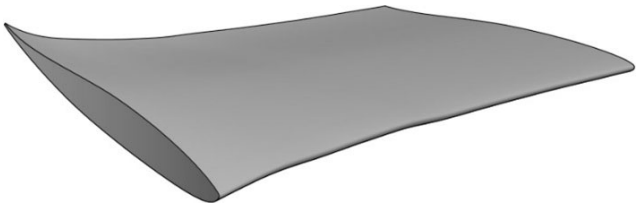

Fig. 15 3D M-fan blade [5]

Fig. 16 2D M-fan airfoil profile at the radius of 2868 mm from the hub center

elements with a minimum orthogonal quality of 0.13 and an average orthogonal quality of 0.96 were used.

5.3 Boundary conditions and solver settings

The airfoil was modelled in the centre of the half circular domain, with a radius of 15 times the chord length, with a prescribed inlet velocity having an x- and y-direction component. The magnitude and direction of the velocity represented the obtained relative velocity and angle of attack at different circumferential positions. The outlet had a boundary condition set to outflow and the airfoil surface had a stationary wall boundary condition. The inlet had a turbulence intensity and dissipation length scale set to the same order of magnitude as that of the facility being emulated. The turbulence intensity was set to 3% and a length scale of 0.02 was used, representing the 20 mm thick walking grid located downstream of the fan. The Spalart Allmaras turbulence model was used for all 2D airfoil simulations [15]. The Spalart Allmaras turbulence model is a one-equation model that solves the

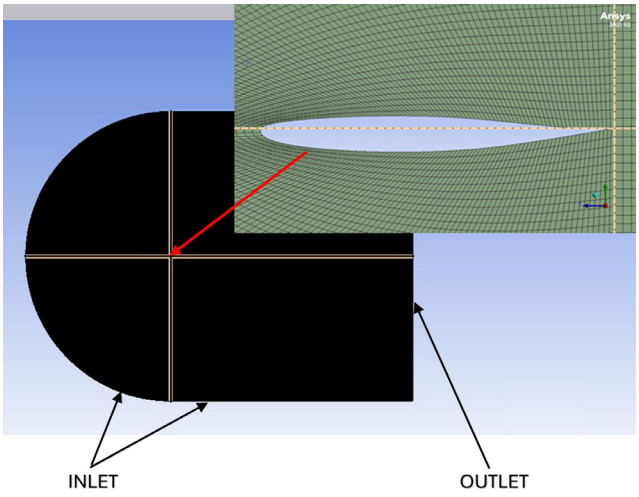

Fig. 17 Lay-out of CFD-model for airfoil analysis

transport equation for turbulent viscosity. This turbulence model is well suited for solving aerodynamic models with adverse pressure gradients and high Reynolds numbers.

5.4 Static pressure data collection

The simulation allowed static pressure data to be gathered over the entire airfoil profile (Fig. 18). This data can further be extracted per *x-y* co-ordinate to find the exact location of the sensors as described in Section 2.4. Fig. 18 was captured at an AoA of 0.63° and a relative velocity of 43.7 m/s.

6 Results

From the results of Thiry [8] a collection of values obtained during the experimental testing of the facility, as well as the numerical analysis of the MinwaterCSP facility are shown. Two parts were analyzed, namely: inlet velocity distribution and blade surface pressure values.

6.1 Experimental inlet velocity distribution

During the operation of the facility, the flow distribution upstream of the M-fan was determined by using the propeller anemometers attached to the rotating beam at a louvre opening setting of 100% and a fan rotational speed set to 151 rpm (see Fig. 19). The average flow rate through the MinwaterCSP facility was 317.85 m^3/s, giving an average inlet velocity of 7.4 m/s. The actual achieved fan rotational speed was 148.95 m/s.

Two different regions of higher inlet velocity were noticed. The higher inlet velocity regions corresponded to the location of the canal running beneath the facility. Therefore it could be concluded that the influence on the velocity profile is caused by the canal. It was believed that the velocity increment is caused due to the greater inlet area present by the canal cavity.

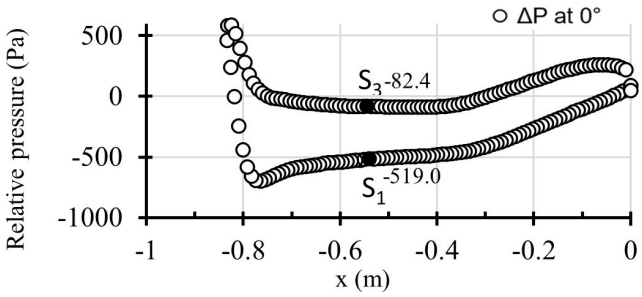

Fig. 18 Relative surface pressure at the radius of 2868 mm from hub to center for circumferential position at 0°

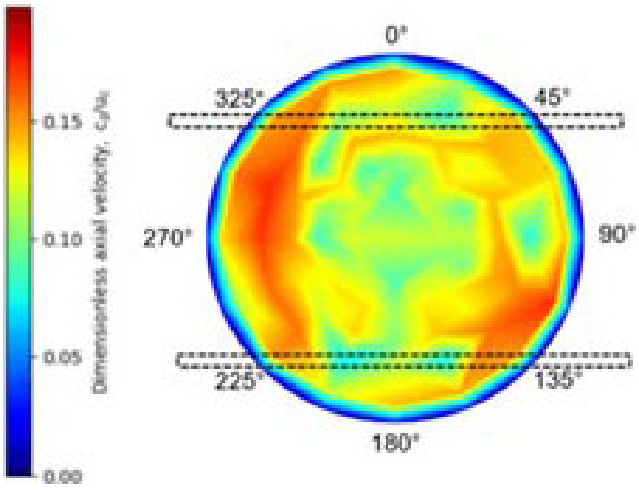

Fig. 19 Velocity distribution upstream of fan rotor

6.2 Simulated inlet velocity distribution

Section 6.2 reports the numerical result for a mass flow rate of 317.85 m^3/s. Fig. 20 (a) indicates the flow field present through the fan. Only half views of the planes are shown. It can be observed in the velocity distribution that the form of the canal affects the distribution. It was noticeable that due to the actuator disk having a large hub diameter, it acted as a bluff body and caused a strong downstream recirculation zone. Pressure loss downstream of the fan's hub is caused by Karman vortices that are released as a function of the rotational speed of the fan. The sharp edges of the rotor disk and the fan geometry enhanced the unsteadiness of the flow. Although the configuration of the rotor disk is motivated by practical reasons involving the manufacturing and installation of such a large diameter

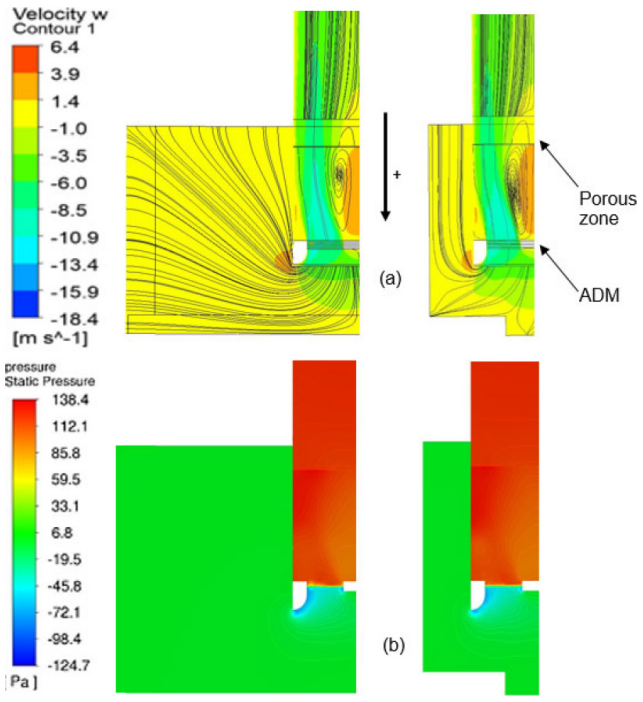

Fig. 20 Velocity (a) and relative pressure (b) of the MinwaterCSP test facility at 317 m^3/s

fan, the effects thereof were investigated experimentally by Wilkinson et al. [5]. The investigation showed that the hub affected the local flow pattern but that the effect on overall performance of the fan at its design point was minimal. The ADM was responsible for the discontinuity in the pressure field present in Fig. 20 (b) and for a higher local flow velocity. Straightening of the flow close to the exit downstream of the fan was caused by the porous zone inserted in the simulations to replicate the grid present in the MinwaterCSP facility. The shape of the bell mouth was modelled to correspond the installed bell mouth of the MinwaterCSP facility. The bell mouth was specifically lengthened to suit the installation of the slew bearing and torque arm configuration consequently causing the separation of the flow field.

The three-dimensional velocities on the upstream and downstream disks were extruded to calculate the relative velocity needed for the 2D simulation analysis. The relative velocity for this two-dimensional simulation was calculated at the flow rate of 317.85 m^3/s. The angle of attack (AoA) and relative velocity were calculated at 8 different locations, every 45° in the actuator disk plane. The different calculated reference velocities allowed the 2D airfoil to be simulated to obtain different surface pressures at the three sensor positions every 45° (see Fig. 21).

The relative pressure distribution around the airfoil for position 1 and 3 at circumferential position 0° with a relative velocity of 43.68 m/s and an AoA of 0.63° is shown in Fig. 22.

6.3 Surface pressure distribution

A summary of the average values of the relative surface pressures results (expressed in Pa), obtained from the experimental and numerical system for the three different

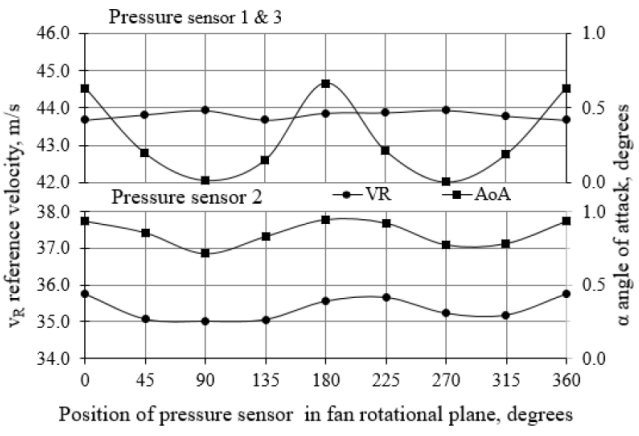

Fig. 21 Relative velocity and angle of attack for pressure sensor positions in fan rotational plane

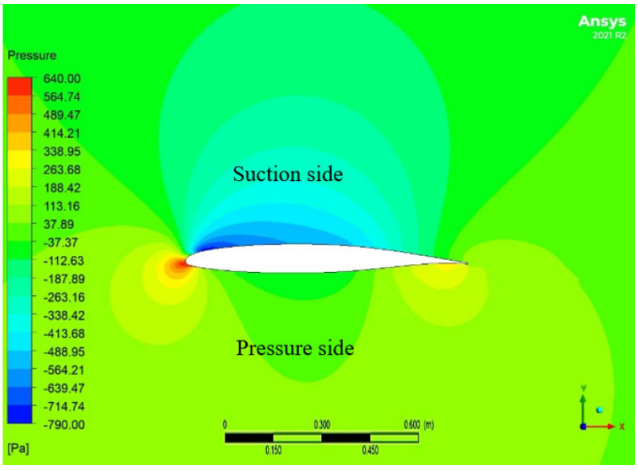

Fig. 22 Relative pressure distribution around airfoil for radial position 1 and 3 for circumferential position 0°

positions, namely position 1, 2 and 3 is shown in Table 4. The relative surface pressure distribution over the fan rotational plane is tabulated in Table 5 and visually represented in Fig. 23.

The simulation and experimental results at sensor position 1 and 2 on the suction side of the blade showed an oscillating shape in the relative blade surface pressure distribution with troughs at 90° and 270° corresponding to the canal's higher air inlet area. Sensor position 3 on the pressure side of the blade showed troughs at the positions perpendicular to the canal, at 0° and 180°. These results were repeatable and suggested a definite effect from the environment. It is believed in this case that the environmental effect was caused by the canal and all other objects present in the vicinity of the MinwaterCSP test facility. For simplicity the simulation only incorporated the geometry of the canal and buildings in the vicinity of the test

Table 4 Average experimental and simulation relative blade surface pressure

Position	1		2		3	
	Δp	Range	Δp	Range	Δp	Range
Experiment	−480.6	36.0	−353.0	26.0	−49.1	49.5
Simulation	−496.3	38.9	−388.7	26.8	−99.8	31.2
Difference	3.1%	2.9	9.2%	0.8	50.8%	18.3

Table 5 Relative blade surface pressure over the fan rotational plane

Position		0°	90°	180°	270°
1	Experiment	−502.8	−466.8	−497.8	−467.3
	Simulation	−519.0	−482.7	−521.0	−482.1
2	Experiment	−366.0	−346.0	−360.0	−340.0
	Simulation	−402.8	−376.0	−398.7	−383.5
3	Experiment	−48.1	−70.1	−20.6	−65.1
	Simulation	−82.4	−111.5	−80.9	−112.1

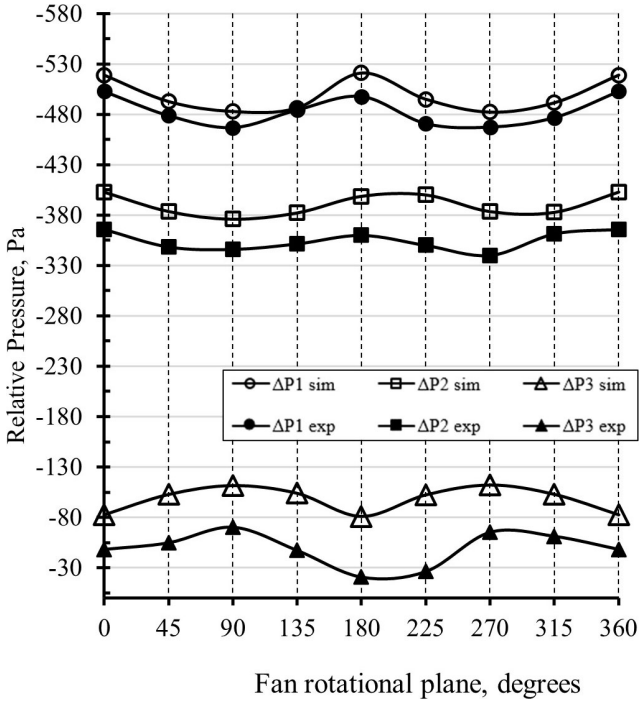

Fig. 23 Relative pressure average over rotational plane

facility, omitting the columns and other objects/structures within the MinwaterCSP test facility.

7 Conclusion

A design procedure to develop a surface pressure measurement application has been developed. The method incorporates a LPS25HB pressure sensing module with an Arduino microcontroller and an XBee telemetry system. This system was installed on to the M-fan blades of the MinwaterCSP facility to capture surface pressure. The goal was to analyse the influence of the canal underneath the facility on the velocity and surface pressure distribution. An oscillating shape was witnessed in the pressure measurement data for all sensing positions. The oscillation for all three sensor positions corresponded well to the canal's location where the velocity distribution was the highest.

A comparative numerical model of the MinwaterCSP facility was created, aided by the use of an actuator disk model (ADM). The numerical models consisted of a three-dimensional representation of the MinwaterCSP facility, including the canal and buildings in the vicinity. The ADM was capable of predicting the flow field in the vicinity of the fan satisfactorily. However in hindsight it was unable to predict any significant influence from the environment on the velocity distribution through the fan. The velocities were extracted and the reference velocities calculated with their correlating angle of attack to simulate the two-dimensional airfoil profiles.

The average relative blade surface pressure values had a difference of 3.1%, 9.2% and 50.8% at position 1, 2 and 3 respectively between the simulation and the experimental result. The average relative pressure range between the simulation and experimental results for position 1, 2 and 3 differed by 2.9 Pa, 0.8 Pa and 18.3 Pa respectively, which falls within the sensor's precision level of 10 Pa.

Within a rotation of the fan, the velocity distribution is non-constant. Locations parallel to the water canal, 90° and 270°, experienced higher axial velocities. Blade element theory correlates a higher axial velocity with a larger average flow angle and therefore a smaller angle of attack. The variation in relative velocity and AoA due to the environment for both experimental and simulation systems caused the relative surface pressure values to oscillate. The 90° out of phase oscillation between sensor position 1, 2 and 3 is due to the effect of a variation in angle of attack at different locations along the blade. Sensor 1 and 2 positioned on the suction side of the blade experience an inverse effect from the higher axial velocities, smaller AoA, whilst sensor position 3 on the pressure side of the blade shows its peaks in relative surface pressure parallel to the canal when influenced by higher reference velocities and smaller angles of attack.

The experimental test clearly showed the influence from the environment on the velocity distribution and surface pressure distribution. The numerical simulation indicated the correct velocity range but did not indicate the same significant influence from the environment on the velocity distribution through the fan. After applying the relative velocity and AoA to the 2D simulation, an accurate resemblance between the simulation and the experimental relative surface pressure distribution was obtained.

8 Recommendations for future research

This study opens avenues for further exploration. Future research could focus on using dimensionless data, performing a Fast Fourier Transform (FFT) on pressure fluctuations, and assessing the impact of lift force fluctuations on blade dynamics.

8.1 Dimensionless data for generalization

To enhance the general applicability of the results and facilitate comparisons with similar studies, future work will present data in a dimensionless format. This approach would benefit fan experts by offering a broader, more generalized interpretation of the results, as highlighted in figures and tables throughout this study.

8.2 FFT analysis of pressure fluctuations

An area for further investigation involves performing an (FFT) analysis on the pressure signals to explore the frequency characteristics of surface pressure fluctuations. This analysis would likely reveal a dominant peak at the rotational frequency, which could be related to the uneven velocity inlet. Additionally, it would be valuable to identify any other characteristic peaks in the frequency spectrum. Conducting this analysis could provide deeper insights into flow behavior and improve our understanding of the fan's operational dynamics.

8.3 Impact of lift force fluctuations on blade dynamics

In future studies, it would be valuable to quantify the extent of lift force fluctuations on the fan blades due to uneven inlet velocity, which affects the angle of attack and creates varying bending moments. These fluctuations could increase the vibration propensity of the blades, potentially leading to operational risks. Analysing and presenting the percentage of blade lift force fluctuation relative to the nominal lift value would serve as a useful indicator of extent of force fluctuations. This analysis could provide valuable insights for fan experts, helping toassess whether such fluctuations pose any operational risks.

Acknowledgement

The financial assistance of the National Research Foundation (NRF) towards this research is hereby acknowledged. Opinions expressed and conclusions arrived at, are those of the author and are not necessarily to be attributed to the NRF.

Nomenclature

D	Drag
F_z	Momentum source term in axial direction
F_q	Momentum source term in tangential direction
K	Pressure loss coefficient
L	Lift
p	Pressure
V	Axial velocity
V_{an}	Anemometer voltage
v_n	Measured velocity
v_c	Calculated velocity
z	Axial distance
β_∞	Flow angle of average velocity vector, relative to plane of rotation
μ	Viscosity
ACC	Air-cooled condenser
ADM	Actuator disc method
AoA	Angle of attack
CFD	Computational fluid dynamics
CSP	Concentrated solar power
FFT	Fast Fourier Transform
PLC	Programmable logic controller
SCADA	Supervisory control and data acquisition
SD	Standard deviation
UDF	User defined function
VAR	Variance

References

[1] MinWaterCSP "MinWaterCSP", [online] Available at: https://minwatercsp.eu/ [Accessed: 15 June 2021]

[2] Kröger, D. G. "Air-cooled Heat Exchangers and Cooling Towers", Pennwell Corporation, 2004. ISBN 9780878148967

[3] van der Spuy, S. J., Els, D. N. J., Tieghi, L., Delibra, G., Corsini, A., Louw, F. G., Zapke, A., Meyer, C. J. "Preliminary Evaluation of the 24 Ft. Diameter Fan Performance In the MinwaterCSP Large Cooling Systems Test Facility", In: ASME Turbo Expo 2021: Turbomachinery Technical Conference and Exposition, 2021, GT2021-59130. ISBN 978-0-7918-8489-8 https://doi.org/10.1115/GT2021-59130

[4] Ma, H., Cai, N., Cai, L., Si, F. "Effects of the forced convection induced by assistant fans on the thermal performance of an indirect dry cooling system", Case Studies in Thermal Engineering, 35, 102141, 2022. https://doi.org/10.1016/j.csite.2022.102141

[5] Wilkinson, M. B. van der Spuy, S. J., von Backström, T. W. "The Design of a Large Diameter Axial Flow Fan for Air-Cooled Heat Exchanger Applications", In: ASME Turbo Expo 2017: Turbomachinery Technical Conference and Exposition, Charlotte, NC, USA, 2017, GT2017-63331. ISBN 978-0-7918-5077-0 https://doi.org/10.1115/GT2017-63331

[6] Louw, F. G., Bruneau, P. R. P., von Backström, T. W., van der Spuy, S. J. "The Design of an Axial Flow Fan for Application in Large Air-Cooled Heat Exchangers", In: ASME Turbo Expo 2012: Turbine Technical Conference and Exposition, Copenhagen, Denmark, 2012, GT2012-69733. ISBN 978-0-7918-4469-4 https://doi.org/10.1115/GT2012-69733

[7] Hurault, J., Kouidri, S., Bakir, F. "Experimental investigations on the wall pressure measurement on the blade of axial flow fans", Experimental Thermal and Fluid Science, 40, pp. 29–37, 2012. https://doi.org/10.1016/j.expthermflusci.2012.01.018

[8] Thiry, C. C. "Measuring the installed performance of the 24 ft diameter MinwaterCSP fan", Master Thesis, Stellenbosch University, 2023.

[9] Muiyser, J. "Simultaneous Measurement of Air Flow Conditions and the Resultant Blade and Gearbox Loading at Large-Scale Cooling System Fans", Master Thesis, Stellenbosch University, 2012.

[10] ANSYS, Inc. "ANSYS Fluent: Fluid Simulation Software, (2021 R2)", [computer program] Available at: https://www.ansys.com/products/fluids/ansys-fluent [Accessed: 30 August 2021]

[11] Thiart, G. D., von Backström, T. W. "Numerical simulation of the flow field near an axial flow fan operating under distorted inflow conditions", Journal of Wind Engineering and Industrial Aerodynamics, 45(2), pp. 189–214, 1993. https://doi.org/10.1016/0167-6105(93)90270-X

[12] Meyer, C. J., Kröger, D. G. "Numerical simulation of the flow field in the vicinity of an axial flow fan", International Journal for Numerical Methods in Fluids, 36(8), pp. 947–969, 2001. https://doi.org/10.1002/fld.161

[13] Shih, T.-H., Liou, W. W., Shabbir, A., Yang, Z., Shu, J. "A new k-ϵ eddy viscosity model for high Reynolds number turbulent flows", Computer & Fluids, 24(3), pp. 227–238, 1995. https://doi.org/10.1016/0045-7930(94)00032-T

[14] van der Spuy, S. J., von Backström, T. W. "An evaluation of simplified CFD models applied to perimeter fans in air-cooled steam condenser", Proceedings of the Institution of Mechanical Engineers, Part A: Journal of Power and Energy, 229(8), pp. 948–967, 2015. https://doi.org/10.1177/0957650915594073

[15] Spalart, P. R., Allmaras, S. R. "A one-equation turbulence model for aerodynamic flows", La Recherche Aérospatiale, 1, pp. 5–21, 1994.